

CXR-LLaVA: Multimodal Large Language Model for Interpreting Chest X-ray Images

Seowoo Lee, M.D.¹, Jiwon Youn², Mansu Kim Ph.D. ^{2†}, Soon Ho Yoon, M.D. Ph.D.^{1†}

¹Department of Radiology, Seoul National University College of Medicine, Seoul National University Hospital, Seoul, Republic of Korea.

² AI Graduate School, Gwangju Institute of Science and Technology, Gwangju, Republic of Korea.

†Co-corresponding authors.

Co-correspondences:

Mansu Kim, Ph.D.

AI Graduate School, Gwangju Institute of Science and Technology (GIST), Gwangju, Republic of Korea.

Email: mansu.kim@gist.ac.kr

Soon Ho Yoon, M.D., Ph.D.

Department of Radiology, Seoul National University College of Medicine, Seoul National University Hospital, Republic of Korea.

Email: yshoka@snu.ac.kr

Type of manuscript: Original Research

Word count for text: 3000

Funding: This work was partly supported by Institute of Information and Communications Technology Planning and Evaluation (IITP) grant funded by the Korea government (MSIT) [No.2019-0-01842, Artificial Intelligence Graduate School Program (GIST), No. 2021-0-02068, Artificial Intelligence Innovation Hub], the National Research Foundation of Korea under grant NRF-2022R1F1A1068529.

Conflicts of Interest: Outside of this work, Soon Ho Yoon works in MEDICAL IP as a chief medical officer and has a stock option of the firm. Other authors have no conflict of interest to declare.

CXR-LLaVA: Multimodal Large Language Model for Interpreting Chest X-ray Images

Manuscript type: Original Research

Summary Statement:

CXR-LLaVA, an open-source multimodal large language model for chest X-ray interpretation, was introduced and validated, demonstrating enhanced performance through prompt engineering and parameter adjustments.

Key Points:

- The model secured an average F1 score of 0.30 for diagnosing five pathologic findings: atelectasis, cardiomegaly, consolidation, edema, and pleural effusion. This score improved to 0.46 with prompt engineering.
- Highlighting its zero-shot capabilities, the model achieved an F1 score of 0.85 when identifying abnormal radiographs in a pediatric chest x-ray dataset. When presented with a prompt about cautiously interpreting cardiomegaly in pediatric chest radiographs, the model's decisions were significantly influenced.

Abstract

Purpose: Recent advancements in large language models (LLMs) have expanded their capabilities in a multimodal fashion, potentially replicating the image interpretation of human radiologists. This study aimed to develop open-source multimodal large language model for interpreting chest X-ray images (CXR-LLaVA). We also examined the effect of prompt engineering and model parameters such as temperature and nucleus sampling.

Materials and Methods: For training, we collected 659,287 publicly available CXRs: 417,336 CXRs had labels for certain radiographic abnormalities (dataset 1); 241,951 CXRs provided free-text radiology reports (dataset 2). After pre-training the Resnet50 as an image encoder, the contrastive language-image pre-training was used to align CXRs and corresponding radiographic abnormalities. Then, the Large Language Model Meta AI-2 was fine-tuned using dataset 2, which were refined using GPT-4, with generating various question answering scenarios. The code can be found at https://github.com/ECOFRI/CXR_LLaVA.

Results: In the test set, we observed that the model's performance fluctuated based on its parameters. On average, it achieved F1 score of 0.34 for five pathologic findings (atelectasis, cardiomegaly, consolidation, edema, and pleural effusion), which was improved to 0.46 through prompt engineering. In the independent set, the model achieved an average F1 score of 0.30 for the same pathologic findings. Notably, for the pediatric chest radiograph dataset—which was unseen during training—the model differentiated abnormal radiographs with an F1 score ranging from 0.84 to 0.85.

Conclusion: CXR-LLaVA demonstrates promising potential in CXR interpretation. Both prompt engineering and model parameter adjustments can play pivotal roles in interpreting CXRs.

Introduction

Advancements in deep learning, marked by the emergence of convolutional neural networks (CNNs) and vision transformers (ViTs), have profoundly impacted radiology (1-3). Many CNN algorithms have transitioned from research to practical implementation. However, while CNNs and ViTs are adept at specific tasks like classification and segmentation, and this specialization could limit their ability to address multifaceted challenges in areas such as radiology.

Simultaneously, the domain of natural language processing has seen breakthroughs, enabling models to adeptly understand and generate human-like text. As these models evolve, they have achieved unprecedented levels of performance, a trend accentuated by the upscaling of models, resulting in "large language models" (LLMs). Models like ChatGPT, with their billions or even trillions of parameters, are showcasing prowess in various linguistic tasks, from text generation to translation (4). Their versatility spans numerous sectors, from healthcare to education, highlighting their wide-ranging potential.

Moving past traditional CNNs, initiatives to integrate imagery with natural language have met with success. Notable models like the contrastive language-image pre-training (CLIP) have set benchmarks in object recognition from images (5). The bootstrapping language-image pre-training (BLIP-2) model in 2023 has reached a level where it can read the context within images and generate detailed captions (6). Meanwhile, the Large Language and Vision Assistant (LLaVA), blending vision encoding with LLM, has achieved top-tier results across diverse visual tasks (7).

Most LLMs typically process and produce text, but many medical tasks, especially in radiology, demand a multimodal approach. This underscores the urgency to devise model's adaptation to both text and other modalities, such as images. Industry leaders like OpenAI and Google have introduced multimodal foundation models, preliminary studies have made attempts at applying them to chest X-ray (CXR) interpretation (8, 9). Yet, the specific uses of these models in radiology remain publicly inaccessible.

A significant facet of LLMs is their sensitivity to hyperparameters like ‘top_p’ and ‘model temperature’. ‘top_p’, or nucleus sampling, controls the randomness of the model's output by focusing on the most probable next words, while model temperature adjusts the model's certainty in its predictions. A lower temperature makes the model more deterministic and confident, while a higher value encourages more diversity in outputs. Furthermore, prompt engineering has emerged as a vital technique to guide and refine the outputs of LLMs (10). By crafting effective prompts, one can harness the model's knowledge and capabilities more effectively, steering it towards desired outputs, especially in complex domains like medical interpretation.

Therefore, this study aims to develop a multimodal large language model for CXR interpretation, while exploring the effects of prompt engineering and model parameters.

Materials and Methods.

This study solely used publicly available datasets and did not require the approval of an institutional review board.

Data collection

For model training, we include several public CXR datasets, collecting a total of 659,287 frontal CXRs as shown in Table 1. Only the Medical Information Mart for Intensive Care (MIMIC) dataset provides radiologic reports in a free-text form (dataset 1, n=241,951), while the other training datasets have multi-class or binary labeling for radiographic abnormalities (dataset 2, n=417,336). Although some datasets contain information regarding the location of lesions, this location information is not utilized.

Adapting Multimodal Large Language Model on CXR Images (CXR-LLaVA)

The model developed in this research largely adopts ideas from the LLaVA network (7). LLaVA is an extended version of LLM, where the token sequence from image encoder is combined with query text tokens for text generation in the LLM. Our primary goal is to leverage biomedical image-text pairs to fine-tune LLaVA. To train biomedical images (i.e., CXR) effectively, we employ a convolutional neural network, specifically Resnet50 instead of a vision transformer as an image encoder and utilizes a single image vector instead of an image token sequence. Similar to LLaVA, we also employ the Large Language Model Meta AI (LLAMA)-2 model as a language model (11). Specifically, among several types of LLAMA-2 models based on parameter size, the 13 billion parameters-sized model was utilized due to cost considerations.

Finally, the CXR-LLaVA takes a CXR image and question text as input; the image is transformed into an image vector via an image encoder, and the question text is converted to text

tokens through a tokenizer. Both are then fed into a causal language model, which autoregressively generates text responses to the questions. The trained model is available as an open source (https://github.com/ECOFRI/CXR_LLaVA), and its demo can be found on <https://radiologist.app/cxr-llava>.

Step1. Constructing and training image encoder specific for CXR

Despite the capabilities of convolutional neural networks in open-world visual understanding, they often fall short in accurately describing radiographic findings. In this section, we propose an image encoder, $f(\mathbf{x})$, based on ResNet-50 and two step strategies for training them to learn radiological context specific for CXR images.

In first step, the simple classification task is used to train image encoder. The image encoder transforms CXR image (\mathbf{x}_{img}) into the representation (\mathbf{z}_{img}) and then classify abnormality (\mathbf{y}) by adding simply fully connected layer as classifier (i.e., $\mathbf{y} = \mathbf{g}(\mathbf{z}_{img})$). We believe that the classification task enable model to learn a fundamental yet crucial ability regarding abnormality. Specifically, we have used 344,091 image-label pairs from the dataset 1 to train our image encoder. We assign binary labels: when images have labels associated with pathology, they are labeled as "abnormal," while those marked as "no finding" are designated "normal." Images with only support devices and no associated pathology labels are excluded, especially when their clinical significance is unclear. The detail implementation and settings are described in supplementary material.

In the second step, the image encoder, $f(\mathbf{x}_{img})$, is trained additionally based on the CLIP strategy, to learn complex representations of radiological term. (5) Specifically, the image encoder, $f(\mathbf{x}_{img})$, and pretrained text encoder, $h(\mathbf{x}_{text}^k)$, from prior research (12) are employed to compute the contrastive loss between image vector (\mathbf{z}_{img}) and text vectors (\mathbf{z}_{text}^k) (i.e., $\mathbf{z}_{img} = f(\mathbf{x}_{img})$ and $\mathbf{z}_{text} = h(\mathbf{x}_{text}^k)$). In our study, we choose k keywords as \mathbf{x}_{text}^k , such as "atelectasis", "pneumonia", and etc. Using CLIP method, the Image encoder enables to learn shared representations between images and text by mapping corresponding image and text pairs closer, and non-corresponding ones

further apart. The 659,287 image-text pairs from the dataset 1 and 2 are used on the training process, the detailed process are described in the supplementary material.

After completing the complex training process, we believe that our image encoder enables to not only perform simple classification but also understand and interpret the medical imagery by bridging the gap between visual data and textual descriptions, potentially advancing diagnostic accuracy and efficiency.

Step 2. Feature Alignment and end-to-end fine tuning of CXR-LLaVA

Before fine-tuning the CXR-LLaVa model, the features from the image encoder, as described in step. 1, and language model (i.e., LLaMa-2) need to be aligned. To align these features, we conduct the additional training where the image encoder and language model weights are frozen, updating only the projection matrix (\mathbf{P}). The aligned image representation (i.e., $\langle \text{image} \rangle = \mathbf{P} \times \mathbf{z}_{\text{img}}$) are computed by updating \mathbf{P} using CXR images with refined radiologic reports. An example is as follows: “Image+Question”: $\langle \text{image} \rangle / \text{nOffer a brief description of the chest radiograph}$, “Answer”: “The chest radiograph shows large right pleural effusion with adjacent compressive atelectasis.”.

After aligning image features, instruction-tuning is employed to fine tune the CXR-LLaVA. For instruction tuning, we used the refined radiology reports and the multi-turn Q&A dialogues generated by GPT-4. A detailed description is available in the supplementary materials. The multi-turn Q&A dialogues are expansion of the generated the hypothetical question-answer pairs, where the conversation includes detailed locations, differential diagnoses and further radiologic study recommendations. The end-to-end fine-tuning process is conducted to update all trainable weights except image encoder. The overarching aim was to enhance the model's ability not only to interpret CXRs but also to respond to a diverse array of questions regarding CXRs for more nuanced and informative interactions in a clinical setting. Detailed implementations of fine-tuning process are provided in the supplementary material.

Effect of prompt in evaluation in CXR-LLaVA

To evaluate generated radiological report, the corresponding label should be annotated from generated text using CXR-LLaVA. In this study, we used OpenAI GPT-3.5 for annotation. The detailed method is provided in the supplementary document. We analyzed how the model's output varied with three different prompts. First, we queried the model using a 'basic' style prompt. Second, we used a specific prompt that explicitly requested information about certain pathologic labels. Third, we performed multi-turn predictions to ascertain if the answer contains specific labels, instead of just receiving a response from the LLM (Table 2). Due to the model's inherent output randomness, we evaluated it three times with each setting and calculated the average F1 score.

Radiologic report generation performance evaluation

The radiologic report generation performance is evaluated to validate diagnostic performance of the proposed model. The accuracy of generated radiologic report is evaluated in terms of precision, recall, and F1 score in both the test set and an independent set. Specifically, radiologic reports are generated by querying each CXR and question into the proposed. Using GPT-3.5 as a labeler, we determine whether each pathologic finding is mentioned in the response. We then calculate the precision, recall, and f1 score between the predictions and the ground truth for each finding.

In the test set, we use the CheXpert test set, which contains 518 CXR images labeled with 14 pathologic findings: atelectasis, cardiomegaly, consolidation, edema, enlarged cardiomedastinum, fracture, lung lesion, lung opacity, no finding, pleural effusion, pleural other, pneumonia, pneumothorax, and support devices (Supplementary Table 1). These ground truth labels were generated by five radiology specialists (13). Among them, five pathologic findings (atelectasis, cardiomegaly, edema, consolidation, pleural effusion) are selected for evaluation because they are clinically significant and have labels with a sufficient number of positive cases.

Additionally, we monitor shifts in the f1 score while adjusting the model temperature and model top probability to investigate potential differences based on model parameters. Moreover, to gauge the difference in diagnostic performance depending on the prompt, we observed fluctuation in the f1 score as varied the prompt.

In independent set, we employ the dataset from Indiana University, which includes 3,689 frontal chest radiographs. This dataset doesn't have specific labels, but instead contains a radiologic report with impressions and findings. To establish a ground truth, we analyzed the radiologic report using GPT-4 to label whether the core five findings (atelectasis, cardiomegaly, consolidation, edema, pleural effusion) exist (Supplementary Table 2). We queried the model with the CXR and generate responses, then calculated precision, recall, and f1 score for each finding.

Zero Shot Performance Evaluation

To evaluate zero-shot classification capabilities, we employ the pediatric CXR dataset from the University of San Diego. This dataset comprises 624 images from child, binary labeled as abnormal or normal. We also evaluate the accuracy of generated radiologic report in terms of precision, recall, and F1-score. Specifically, the radiologic report is generated by querying each CXR and question into the proposed. The pathologic finding is annotated using GPT-3.5 as a labeler, as described above. In addition, we observe the effect of the prompt, where detail the characteristics of pediatric chest radiographs is incorporated, since the pediatric chest, being relatively small compared to the heart, can sometimes be misinterpreted as showing cardiomegaly (Table 2).

Results

Report generation performance on the test dataset

Table 3 illustrates the model's report generation capabilities on the test dataset. While its overall diagnostic performance does not equate to human radiologists', as established in previous studies, the model's accuracy in detecting atelectasis and cardiomegaly neared the standards set by human experts when the model is optimally configured (14). Figure 1 displays an example chest radiograph, highlighting the appropriate format of the generated radiologic report. This report pinpoints critical findings, but it overlooks details like the central catheter.

Impact of prompt engineering on the test dataset

Table 3 delineates how the model's performance varies on the test dataset based on different prompts and prediction methodologies. When furnished with a basic prompt to create a CXR report, the model's performance tends to falter. Yet, with a specific prompt guiding the model to generate a CXR report emphasizing pathologic findings, its efficiency markedly improves. Following the production of a radiologic report using this specific prompt, subsequent confirmations via multi-turn predictions improved the model's recognition of atelectasis, cardiomegaly, consolidation, and edema. However, the performance metrics concerning pleural effusion remained largely unchanged. It's evident that prompt engineering plays a pivotal role in influencing the model's effectiveness.

Model performance variation based on parameters in the test dataset

The model's performance, influenced by temperature and the nucleus sampling parameter (top_p), is detailed in Supplementary Table 4. In general, a higher top_p correlates with improved results. For the five target labels, the optimal settings were found to be a model temperature of 0.4 and a top_p value of 0.8. This configuration was consistently used across all types of inferences. Due to inherent factors

within the LLM, the output may vary with each inference. We also assessed the consistency of the model's performance across multiple inferences. The standard deviation of the F1 scores ranged from 0.00 to 0.03, and this variability tended to rise with increasing model temperature and top_p values. This suggests that the quality of the model output can fluctuate with each inference, especially when using higher model temperatures and top_p.

Report generation performance on the independent test dataset

In the independent test dataset, the model produced a lower F1 score compared to the internal test set (Table 4). The model showed relatively better results for cardiomegaly, atelectasis, and pleural effusion, but underperformed in consolidation and pulmonary edema. Upon examining a few examples, we can observe that the model appropriately pinpointed and described the essential lesions. Not only was it capable of chest radiograph generation, but it also provided diagnoses and suggested appropriate additional tests (Figure 2-4).

Zero-shot report generation performance on the pediatric independent test dataset

The model achieved a notable F1 score between 0.84-0.85 for diagnosing abnormality, even on a pediatric dataset that it hadn't encountered during training. Interestingly, after adding a prompt advising caution when diagnosing cardiomegaly in pediatric CXRs, the proportion of CXRs that the model diagnosed as abnormal and mentioned cardiomegaly decreased from 71% to 36%. This indicates that prompts can have a significant impact on the model's performance in detecting pathologies. While the F1 score was largely consistent, the addition of a cautionary note in the prompt about interpreting pediatric CXRs led to a marginal improvement in specificity.

Discussion

In our study, we successfully developed a multimodal LLM for CXR interpretation and explored how LLM parameters influence the performance of radiologic report generation. We discovered that parameters such as prompt, temperature, and nucleus sampling can optimize diagnostic performance. This understanding is vital when integrating LLM-based models into clinical practice. Similar to setting thresholds based on sensitivity and specificity for classification CNNs in clinical environments, LLM-based models necessitate precise configurations for temperature and nucleus sampling parameters. We notably found that the model's performance could be affected by the prompt. This suggests that 'prompt engineering' can enhance the generation of radiology reports. In practice, it's essential to control these parameters, and they may need in-depth scrutiny during approval processes like those by the FDA for medical devices.

The performance of our model was notably lower for the "consolidation" label compared to other labels such as atelectasis, cardiomegaly, edema, and pleural effusion, the latter of which tend to involve larger areas in CXR images. Although several other non-peer-reviewed public multimodal LLMs, including Xraygpt, UniXGen, and LLM-CXR, have been released for CXR interpretation, a direct comparison of their performance with ours wasn't feasible (9, 15, 16). However, it's worth noting that these models, like ours, also demonstrated a low performance for the "consolidation" label. This suggests that current approaches, including our own, have a deficiency in evaluating focal lesions, possibly due to the limited performance capabilities of the image encoder. Interestingly, the latest multimodal LLM for CXR interpretation released by Google in September 2023 demonstrated more consistent performance across all labels (17).

This study has several limitations. Firstly, unlike the neural network from the precedent study which approached the level of human radiologists, the model developed in this study appears not to achieve an f1-score at the level of human radiologists. The most probable reason is that our model does not predict the label directly but instead generates free text. The conversion of the output free text using GPT-3.5 into pathology labels might have led to inaccurate results. For instance, there are

various expressions that can signify "cardiomegaly", ranging from definite phrases like "enlarged heart" or "enlarged cardiac silhouette" to vaguer terms like "enlarged cardiomedastinum", "top normal heart", "worrisome heart size", "somewhat enlarged heart", "upwardly displaced heart apex", and "obscured heart border". The process of binary labeling can result in a significant loss of information, which might explain the inferior performance compared to precedent studies. Moreover, the performance on the independent set was lower than on the test set. Since the independent set lacks labels created by human radiologists, only possessing them in free text format, the two-fold conversion process might have generated imprecise labels, possibly explaining the suboptimal results. In fact, precedent studies evaluating from free-text to labels show lower F1 scores (15, 16).

Another limitation is that our model was designed not just to generate radiologic reports, but also to provide differential diagnoses and recommend whether additional imaging is necessary. Unfortunately, we couldn't assess this. Currently, there seems to be no appropriate dataset to determine the accuracy of specific disease diagnoses from CXRs and the necessity for additional tests. We hope this can be evaluated in subsequent research. Furthermore, we examined the effect of prompt engineering and hyperparameters solely in our model. The degree of effect may vary according to different models and model's performance.

In conclusion, we've demonstrated that using multimodal LLM, we can generate radiologic reports that appropriately recognize major lesions and have identified which parameters might influence this process. We anticipate that LLM-based models hold the potential to assist doctors in interpreting X-ray images in the future.

References

1. Shamshad F, Khan S, Zamir SW, Khan MH, Hayat M, Khan FS, Fu H. Transformers in medical imaging: A survey. *Medical Image Analysis* 2023;102802.
2. Huang S-C, Pareek A, Jensen M, Lungren MP, Yeung S, Chaudhari AS. Self-supervised learning for medical image classification: a systematic review and implementation guidelines. *NPJ Digital Medicine* 2023;6(1):74.
3. Shen D, Wu G, Suk H-I. Deep learning in medical image analysis. *Annual review of biomedical engineering* 2017;19:221-248.
4. Gozalo-Brizuela R, Garrido-Merchan EC. ChatGPT is not all you need. A State of the Art Review of large Generative AI models. *arXiv preprint arXiv:230104655* 2023.
5. Radford A, Kim JW, Hallacy C, Ramesh A, Goh G, Agarwal S, Sastry G, Askell A, Mishkin P, Clark J. Learning transferable visual models from natural language supervision. *International conference on machine learning: PMLR*, 2021; p. 8748-8763.
6. Li J, Li D, Savarese S, Hoi S. Blip-2: Bootstrapping language-image pre-training with frozen image encoders and large language models. *arXiv preprint arXiv:230112597* 2023.
7. Liu H, Li C, Wu Q, Lee YJ. Visual instruction tuning. *arXiv preprint arXiv:230408485* 2023.
8. Tu T, Azizi S, Driess D, Schaekermann M, Amin M, Chang P-C, Carroll A, Lau C, Tanno R, Ktena I. Towards generalist biomedical ai. *arXiv preprint arXiv:230714334* 2023.
9. Thawkar O, Shaker A, Mullappilly SS, Cholakkal H, Anwer RM, Khan S, Laaksonen J, Khan FS. Xraygpt: Chest radiographs summarization using medical vision-language models. *arXiv preprint arXiv:230607971* 2023.
10. Liu P, Yuan W, Fu J, Jiang Z, Hayashi H, Neubig G. Pre-train, Prompt, and Predict: A Systematic Survey of Prompting Methods in Natural Language Processing. *ACM Comput Surv* 2023;55(9):Article 195. doi: 10.1145/3560815

11. Touvron H, Martin L, Stone K, Albert P, Almahairi A, Babaei Y, Bashlykov N, Batra S, Bhargava P, Bhosale S. Llama 2: Open foundation and fine-tuned chat models. arXiv preprint arXiv:230709288 2023.
12. Boecking B, Usuyama N, Bannur S, Castro DC, Schwaighofer A, Hyland S, Wetscherek M, Naumann T, Nori A, Alvarez-Valle J. Making the most of text semantics to improve biomedical vision–language processing. European conference on computer vision: Springer, 2022; p. 1-21.
13. Irvin J, Rajpurkar P, Ko M, Yu Y, Ciurea-Ilcus S, Chute C, Marklund H, Haghgoo B, Ball R, Shpanskaya K. Chexpert: A large chest radiograph dataset with uncertainty labels and expert comparison. Proceedings of the AAAI conference on artificial intelligence2019; p. 590-597.
14. Tiu E, Talius E, Patel P, Langlotz CP, Ng AY, Rajpurkar P. Expert-level detection of pathologies from unannotated chest X-ray images via self-supervised learning. Nature Biomedical Engineering 2022;6(12):1399-1406.
15. Lee H, Kim W, Kim J-H, Kim T, Kim J, Sunwoo L, Choi E. Unified Chest X-ray and Radiology Report Generation Model with Multi-view Chest X-rays. arXiv preprint arXiv:230212172 2023.
16. Lee S, Kim WJ, Ye JC. LLM Itself Can Read and Generate CXR Images. arXiv preprint arXiv:230511490 2023.
17. Xu S, Yang L, Kelly C, Sieniek M, Kohlberger T, Ma M, Weng W-H, Kiraly A, Kazemzadeh S, Melamed Z. ELIXR: Towards a general purpose X-ray artificial intelligence system through alignment of large language models and radiology vision encoders. arXiv preprint arXiv:230801317 2023.
18. Signoroni A, Savardi M, Benini S, Adami N, Leonardi R, Gibellini P, Vaccher F, Ravanelli M, Borghesi A, Maroldi R. BS-Net: Learning COVID-19 pneumonia severity on a large chest X-ray dataset. Medical Image Analysis 2021;71:102046.
19. Jaeger S, Candemir S, Antani S, Wang Y-XJ, Lu P-X, Thoma G. Two public chest X-ray datasets for computer-aided screening of pulmonary diseases. Quantitative imaging in medicine and surgery

2014;4(6):475.

20. Wang X, Peng Y, Lu L, Lu Z, Bagheri M, Summers RM. ChestX-ray8: Hospital-scale Chest X-ray Database and Benchmarks on Weakly-Supervised Classification and Localization of Common Thorax Diseases. arXiv:170502315 2017.
21. Bustos A, Pertusa A, Salinas J-M, De La Iglesia-Vaya M. Padchest: A large chest x-ray image dataset with multi-label annotated reports. Medical image analysis 2020;66:101797.
22. Lakhani P, Mongan J, Singhal C, Zhou Q, Andriole KP, Auffermann WF, Prasanna P, Pham T, Peterson M, Bergquist PJ. The 2021 SIIM-FISABIO-RSNA Machine Learning COVID-19 Challenge: Annotation and standard exam classification of COVID-19 chest radiographs. Journal of Digital Imaging 2023;36(1):365-372.
23. Nguyen HQ, Lam K, Le LT, Pham HH, Tran DQ, Nguyen DB, Le DD, Pham CM, Tong HT, Dinh DH. VinDr-CXR: An open dataset of chest X-rays with radiologist's annotations. Scientific Data 2022;9(1):429.
24. Johnson A, Pollard T, Mark R, Berkowitz S, Horng S. MIMIC-CXR Database (version 2.0. 0). PhysioNet. 2019.
25. Johnson AE, Pollard TJ, Berkowitz SJ, Greenbaum NR, Lungren MP, Deng C-y, Mark RG, Horng S. MIMIC-CXR, a de-identified publicly available database of chest radiographs with free-text reports. Scientific data 2019;6(1):317.
26. Demner-Fushman D, Kohli MD, Rosenman MB, Shooshan SE, Rodriguez L, Antani S, Thoma GR, McDonald CJ. Preparing a collection of radiology examinations for distribution and retrieval. Journal of the American Medical Informatics Association 2016;23(2):304-310.
27. Kermany D, Zhang K, Goldbaum M. Labeled optical coherence tomography (oct) and chest x-ray images for classification. Mendeley data 2018;2(2):651.
28. Kermany DS, Goldbaum M, Cai W, Valentim CC, Liang H, Baxter SL, McKeown A, Yang G, Wu

X, Yan F. Identifying medical diagnoses and treatable diseases by image-based deep learning. *cell*
2018;172(5):1122-1131. e1129.

Tables

Table 1. Collection countries, years of publication, and the numbers of frontal chest radiographs in publicly available datasets used for model training and evaluation.

Dataset	Collection Country	Year of Publication	Numbers of Frontal CXRs
Training dataset 1: chest radiograph datasets with pathologic findings labeled			
BrixIA COVID-19 dataset (18)	Italy	2021	4695
CheXpert train/validation dataset (13)			
Montgomery tuberculosis dataset (19)	USA	2014	138
NIH dataset (20)	USA	2017	88337
PadChest dataset (21)	Spain	2019	108048
RSNA COVID-19 AI Detection Challenge(22)	Various countries	2021	6334
Shenzen tuberculosis dataset (19)	China	2014	662
VinDR dataset (23)	Vietnam	2020	17893
<i>Subtotal</i>			417336
Training dataset 2: chest radiograph dataset with free-text radiologic reports			
MIMIC dataset (24, 25)	USA	2019	241951
Test set			
CheXpert test dataset (13)	USA	2022	518
Independent test sets			
Indiana University dataset (26)	USA	2016	3689
San Diego University pediatric dataset (27, 28)	USA	2017	624

Table 2. List of prompts used during the model inference process. We queried the model with each prompt and compared the inference results.

Alias	Type	Content0
Basic prompt	Single-turn	Q : “Write a radiologic report on the given chest radiograph.”
Specific prompt	Single-turn	Q : “Write a radiologic report on the given chest radiograph, including information about atelectasis, cardiomegaly, consolidation, pulmonary edema, pleural effusion, and pneumothorax”
Specific prompt with confirmation	Multi-turn	<p>Q : “Write a radiologic report on the given chest radiograph, including information about atelectasis, cardiomegaly, consolidation, pulmonary edema, pleural effusion, and pneumothorax”</p> <p>A : [The model output]</p> <p>Q : “Respond with yes or no. Is there any [cardiomegaly]?”</p>
Specific prompt with a note to be cautious when diagnosing cardiomegaly in pediatric CXRs	Single-turn	<p>Q : “Write a radiologic report on the given chest radiograph, including information about atelectasis, cardiomegaly, consolidation, pulmonary edema, pleural effusion, and pneumothorax.</p> <p><i>Note. In pediatric radiograph, the cardiac shadow might seem larger due to the heart's proportion to the thorax, so one must be cautious when diagnosing cardiomegaly.</i>”</p>

Table 3. Model's performance in the test set based on prompts.

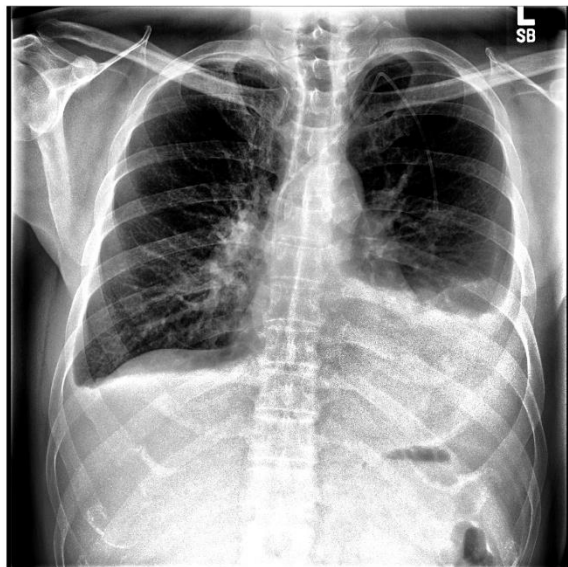
F1 Scores of Each Label					
	Basic prompt	Specific prompt	Specific prompt with confirmation	Improvement in F1 score through prompt engineering	Human radiologists (14)
Atelectasis	0.43±0.04	0.52±0.01	0.59±0.01	0.16	0.69
Cardiomegaly	0.34±0.03	0.47±0.02	0.59±0.01	0.25	0.68
Consolidation	0.09±0.07	0.12±0.04	0.19±0.04	0.10	0.39
Edema	0.31±0.02	0.40±0.03	0.40±0.01	0.09	0.58
Pleural effusion	0.55±0.02	0.49±0.02	0.52±0.01	-0.02	0.74
Average	0.34±0.04	0.40±0.02	0.46±0.02	0.12	0.62

Table 4. Model's performance in the independent test set.

F1 Scores of Each Label		
	Single turn prediction	Multi-turn prediction
	Specific prompt	Specific prompt with confirmation
Atelectasis	0.30±0.02	0.34±0.01
Cardiomegaly	0.42±0.00	0.43±0.02
Consolidation	0.14±0.01	0.11±0.03
Pulmonary edema	0.21±0.01	0.20±0.02
Pleural effusion	0.35±0.00	0.40±0.02
Average	0.29±0.01	0.30±0.02

Figures

Figure 1. An example of a chest radiograph from the test set. While the model identifies the presence of pleural effusions, atelectasis, and lung opacity, it omits details about the central catheter (support device).



[Question] Write a radiologic report on the given chest radiograph, including information about atelectasis, cardiomegaly, consolidation, pulmonary edema, pleural effusion, and pneumothorax.

[Model output] The radiologic report reveals a moderate left pleural effusion. There is also a small right pleural effusion. The cardiomedastinal contours are normal. There is mild vascular congestion present. Opacities in the left lower lobe are consistent with atelectasis.

[Ground truth labels]

Lung Opacity, Atelectasis, Pleural Effusion, Support Devices

Figure 2. An example of a chest radiograph from the independent test set. The model's interpretation includes information about bilateral pulmonary nodules and suggests a possible diagnosis of lung metastasis, which is the correct diagnosis. It also recommends that an additional chest CT scan might be helpful. However, the model could not detect implanted venous access device.



[Question1] Write a radiologic report on the given chest radiograph, including information about atelectasis, cardiomegaly, consolidation, pulmonary edema, pleural effusion, and pneumothorax.

[Model output] The chest radiograph reveals multiple bilateral pulmonary metastases. There is no definite focal consolidation, pleural effusion, or pneumothorax. The cardiomediastinal silhouette is within normal limits.

[Question2] What can be possible diagnosis?

[Model output] The presence of multiple bilateral pulmonary nodules suggests metastatic disease. However, other conditions such as granulomatous diseases, infectious diseases, or benign tumors could also be possible.

[Question3] What kind of further examination is required?

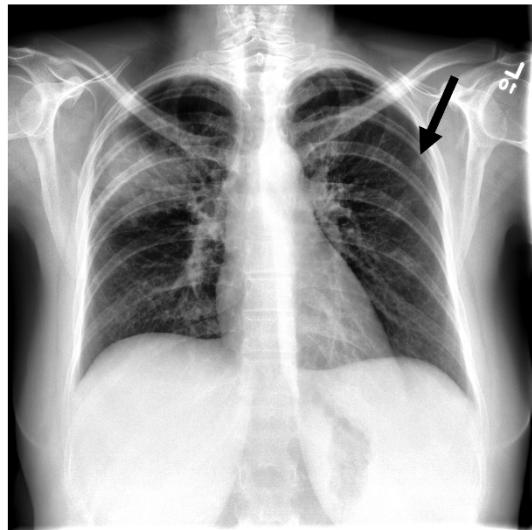
[Model output] Further assessment with a chest CT scan is recommended for better evaluation of the pulmonary nodules.

[Ground truth]

Findings: The heart is normal in size. The mediastinum is stable. Left-sided chest XXXX is again visualized with tip at cavoatrial junction. There is no pneumothorax. Numerous bilateral pulmonary nodules have increased in size and number XXXX compared to prior study. The dominant nodule/mass in the left midlung is also mildly increased. There is no pleural effusion.

Impression : Interval increase in size and number of innumerable bilateral pulmonary nodules consistent with worsening metastatic disease.

Figure 3. An example of a chest radiograph from the independent test set. The model's interpretation identifies right upper lobe pneumonia and proposes a lung abscess as a differential diagnosis, which, while less probable, is reasonable. Nonetheless, the model failed to detect a small left upper lung nodule (black arrow).



[Question1] Write a radiologic report on the given chest radiograph, including information about atelectasis, cardiomegaly, consolidation, pulmonary edema, pleural effusion, and pneumothorax.

[Model output] The chest radiograph reveals a right upper lobe pneumonia. There is no evidence of pleural effusion or pneumothorax. The cardiomedastinal and hilar silhouettes are of normal size.

[Question2] Could there be an alternative diagnosis besides pneumonia?

[Model output] Yes, another differential diagnosis could be lung abscess.

[Question3] What kind of further examination is required?

[Model output] A follow-up chest radiograph is recommended to document substantial clearing of the pneumonia.

[Ground truth]

Findings: The cardiomedastinal silhouette and vasculature are within normal limits for size and contour. There is right upper lobe airspace disease. There is a rounded nodular opacity in the left upper lung measuring approximately 7 mm which may represent further sequela of infectious process versus other pathology. Osseous structures are within normal limits for patient age.

Impression: 1. Right upper lobe pneumonia. 2. Rounded nodular opacity in the peripheral left upper lung which may represent further sequela infectious process versus other pathology including metastatic disease in a patient with thyroid cancer. Follow up to resolution recommended.

Figure 4. An example of a chest radiograph from the independent test set. The model's interpretation identifies bilateral pulmonary opacification and cardiomegaly. Additionally, the model suggests pulmonary edema as the primary diagnosis, which is appropriate.



[Question] Write a radiologic report on the given chest radiograph, including information about atelectasis, cardiomegaly, consolidation, pulmonary edema, pleural effusion, and pneumothorax.

[Model output] The chest radiograph reveals diffuse bilateral pulmonary opacifications. The cardiac silhouette is enlarged, which likely represents pulmonary edema. However, in the appropriate clinical setting, the diffuse alveolar opacities could reflect widespread pneumonia or even ARDS.

[Ground truth]

Findings: The heart is enlarged. There is pulmonary vascular congestion with diffusely increased interstitial and mild patchy airspace opacities. The distribution XXXX pulmonary edema. There is no pneumothorax or large pleural effusion. There are no acute bony findings.

Impression: Cardiomegaly with vascular congestion and suspected pulmonary edema.

[This page intentionally left blank.]

Acknowledgements

We appreciate the high-performance GPU computing support of HPC-AI Open Infrastructure via GIST SCENT. We also acknowledge the utilization of LLM (gpt-4, OpenAI) to enhance the quality of our medical writing. Any revisions made by LLM was thoroughly reviewed by the authors and subsequent adjustment were made as deemed appropriate.

This work was partly supported by Institute of Information and Communications Technology Planning and Evaluation (IITP) grant funded by the Korea government (MSIT) [No.2019-0-01842, Artificial Intelligence Graduate School Program (GIST), No. 2021-0-02068, Artificial Intelligence Innovation Hub], the National Research Foundation of Korea under grant NRF-2022R1F1A1068529.

Supplementary Materials

Detailed Architecture and Training Process of the CXR Image Encoder

We have developed a CXR image encoder utilizing the Resnet50 architecture [1]. Notably, the proposed image encoder comprises 50 residual network blocks, integrating an attention pooling layer instead of the conventional global average pooling layer [2]. Following the training process, this image encoder transforms CXR images (i.e., those with dimensions of 512x512 and RGB channels) into a 1024-dimensional representation vector, which is subsequently employed for further analysis. Our approach employs a two-staged training strategy to impart radiological context..

In the initial training phase, we first pretrain the image encoder for distinguishing between normal and abnormal. This is accomplished by adding a dense binary classifier to the image encoder. Specifically, we used the dataset 1 in this step and implementation details are described as following. The model is initialized with weights pre-trained on the ImageNet dataset. It was trained up to 100 epochs with a learning rate of 1e-3 using the SGD optimizer and a batch size of 64. Training took about one week with a single NVIDIA A100. The final model was chosen based on the lowest validation loss, and the trained model showed an AUROC of approximately 0.92 for the binary classification task.

Subsequent to the initial training phase, we incorporate the CLIP (Contrastive Language-Image Pretraining) method to further enhance the image encoder's ability to understand the relationship between text and CXR images. Specifically, we utilize a text encoder based on the Bidirectional Encoder Representations from Transformers (BERT) from prior research. [3] The trained image encoder was then integrated and trained to minimize the contrastive loss between the image vector and text vector. In this step, we trained them twice with different dataset (dataset 1 and 2). In the initial training stage with dataset 1, we used pathology labels which did not contain location information to learn representation. To accelerate the learning speed, the text encoder was frozen up to step 70k, and then it was unfrozen and training continued. A learning rate of 0.005 with an SGD optimizer was used during this phase, and it took about a day using eight NVIDIA A100s. Training was halted when the validation loss reached a plateau. In the subsequent training stage with dataset 2, refined radiologic reports, which contain not only pathology but also the locations of the pathology, were used to learn the relationship between text and CXR images. The method to refine these reports is discussed in the following section. The model with the lowest validation loss was finally chosen. A quantitative analysis of the CLIP model's performance was not conducted.

Detailed Architecture and Training Process of the CXR-LLaVA.

We adopted the idea of LLaVA. [4] CXR-LLaVA is composed of the image encoder trained in the previous process, a multimodal projection layer, and LLAMA2. When a text prompt and CXR are input into this model, the LLAMA2 tokenizer first converts the text prompt into a vector. Meanwhile, the image encoder processes the CXR to produce a 1024-dimensional vector. This vector is then transformed into a 5120-dimensional vector through the dense multimodal projection layer. This 5120-dimensional vector is inserted into the specified location of the text prompt, and, when it's fed autoregressively into the causal LLM, a response is generated

The training process for CXR-LLaVA occurred in two stages. In the first stage, all layers except the multimodal projection layer were frozen, and training proceeded to align the image vector and text vector spaces. This phase was executed for 1 epoch using a learning rate of 2e-3 with the Adam optimizer, a batch size of 16, and took about 1 hour on eight NVIDIA A100 40GB GPUs. In the second stage, only the image encoder was frozen while all other layers were set to be trainable, and the training continued. This was done for 3 epochs with a learning rate of 2e-5 using the Adam optimizer, a batch size of 16, and took approximately 50 hours on eight NVIDIA A100 40GB GPUs. No validation was conducted during the CXR-LLaVA training process, and the final model was chosen as the ultimate model.

Refining the Radiologic Report and Preparing the LLM Fine-Tuning Dataset

The MIMIC dataset provides free-text radiology reports for CXRs. However, original radiology reports are not suitable for use as training data since they contain contextual information that cannot be inferred from a single CXR, like comparisons with previous images and the patient's medical history. We used OpenAI GPT-4 to remove such parts, and the prompt we used is as follows:

You are skillful radiologist and doing summarization of chest x-ray report.
Summarize these information from the report.
Answer to each questions as json format which have "standard report", "conclusion" and "recommendation" as keys.

1. "standard_report" : Write a standardized radiologic report as one paragraph. Standardized report must include information about abnormality of lungs, mediastinum, heart and thorax.
2. "conclusion" : What is the conclusion or impression of the radiologic report? Include only critical information.
3. "recommendation" : Should additional radiologic study needed? What type of study should be performed?

Do not include any temporal or time information in standard_report and conclusion. DO NOT USE WORD SUCH AS "new", "previous", "comparison", "stable", "improved", "improving", "decreased", "increased", "changed", "unchanged", "resolved", or "cleared".
Do not include information about 'comparison with prior study'.
Do not include information about lateral radiograph.
Replace any numeric information, such as millimeter or centimeter
Remove any information about patient age, gender, and medical history.
Remove any under-bar & blank.
Remove any information or location about catheter, chest tube, endotracheal tube, PICC, chemoport, central line, nasogastric tube or other medical devices.

In addition to simply generating radiologic report, we also created a Q&A dataset for each chest radiograph to incorporate a question answering feature as follows:

"question1" : Compose a question from the perspective of a student radiologist, inquiring about the anatomical location, number, or presence of pathology in the chest radiograph.
"answer1" : Write an informative answer to question1.
"question2" : Compose a question that asks possible differential diagnoses from this chest radiograph, without referring to the patient's history.
"answer2" : Write an informative answer to question2.

Generating Labels from Radiologic Reports

We used OpenAI GPT-3.5 to label pathologies from radiologic reports. The prompt is provided below.

Read the radiologic report of the chest radiograph carefully and determine the existence of the pathologic findings listed below. The output must be a JSON-formatted dictionary with boolean values, using the pathologic categories as keys.

Pathologic categories:

- Cardiomegaly
- Edema
- Consolidation
- Atelectasis
- Pleural Effusion
- No Finding

REPORT: <RADIOLOGIC REPORT GENERATED BY MODEL>

To make the model's output deterministic, we set the GPT model's temperature to zero.

Label Distribution in the Test Set

The CheXpert test dataset provides labels for 14 findings. Their distribution is as follows:

	Negative	Positive
Atelectasis	360	158
Cardiomegaly	364	154
Consolidation	489	29
Edema	439	79
Enlarged Cardiomediastinum	262	256
Fracture	513	5
Lung Lesion	509	9
Lung Opacity	246	272
No Finding	450	68
Pleural Effusion	413	105
Pleural Other	518	0
Pneumonia	507	11
Support Devices	252	266
No Finding	450	68

Table 1. Label distribution in the test set

Among them, five pathologic findings (atelectasis, cardiomegaly, edema, consolidation, pleural effusion) were selected for evaluation. These findings were deemed clinically significant, believed to have a sufficient number of positive cases, and were also emphasized in evaluations in prior study that used the same dataset for assessment purposes. [5]

Label Distribution in the Independent Set

The Indiana University dataset provides free-text radiology reports. We extracted labels from radiology reports using GPT-4 for five pathological findings: atelectasis, cardiomegaly, edema, consolidation, and pleural effusion. Their distribution is as follows:

	Negative	Positive
Atelectasis	3344	345
Cardiomegaly	3348	341
Consolidation	3542	147
Edema	3618	71
Pleural Effusion	3500	189

Table 2. Label distribution in the independent test set

Label Distribution in the pediatric independent test set

The San Diego University pediatric independent test set provides a binary label: abnormal vs. normal. The distribution is as follows:

	Numbers of data
Normal	234
Abnormal	390

Table 3. Label distribution in the pediatric independent test set

Model Performance Variation Based on Model Temperature and Nucleus Sampling Parameter

The LLM has parameters for temperature and nucleus sampling. To determine which conditions are optimal, we varied the model temperature and top_p and calculated the f1-score for each finding on the internal test set. When calculating the average f1-score for the five key findings, the best f1 score was achieved with a temperature of 0.4 and top_p of 0.8.

Mean F1 score for the five conditions: Atelectasis, Cardiomegaly, Consolidation, Edema, and Pleural effusion							
		Model temperature					
	F1-score	0	0.2	0.4	0.6	0.8	1
Top_p	0.2	0.366	0.357	0.357	0.363	0.359	0.352
	0.5	0.368	0.360	0.368	0.368	0.373	0.373
	0.8	0.368	0.375	0.398	0.394	0.387	0.359

Standard deviation of mean F1 scores during model inferences on five conditions: Atelectasis, Cardiomegaly, Consolidation, Edema, and Pleural effusion							
		Model temperature					
	F1-score	0	0.2	0.4	0.6	0.8	1
Top_p	0.2	0.0005	0.0013	0.0003	0.0004	0.0035	0.0098
	0.5	0.0028	0.0133	0.0142	0.0191	0.0232	0.0233
	0.8	0.0029	0.0169	0.0243	0.0207	0.0299	0.0291

Table 4. Model performance variation based on model temperature and nucleus sampling parameter

Model's Performance in the pediatric independent test set

	Specific prompt	Specific prompt with a note to be cautious when diagnosing cardiomegaly in pediatric CXRs.
F1 score	0.85 ± 0.004	0.84 ± 0.01
Sensitivity	0.97 ± 0.01	0.92 ± 0.004
Specificity	0.47 ± 0.01	0.53 ± 0.03
The proportion of CXRs that the model diagnosed as 'abnormal' and also identified as having 'cardiomegaly'.	0.71 ± 0.01	0.36 ± 0.01

Table 5. Model's performance in the pediatric independent test set

References

1. He, K., et al. *Deep residual learning for image recognition*. in *Proceedings of the IEEE conference on computer vision and pattern recognition*. 2016.
2. Radford, A., et al. *Learning transferable visual models from natural language supervision*. in *International conference on machine learning*. 2021. PMLR.
3. Boecking, B., et al. *Making the most of text semantics to improve biomedical vision–language processing*. in *European conference on computer vision*. 2022. Springer.
4. Liu, H., et al., *Visual instruction tuning*. arXiv preprint arXiv:2304.08485, 2023.
5. Tiu, E., et al., *Expert-level detection of pathologies from unannotated chest X-ray images via self-supervised learning*. *Nature Biomedical Engineering*, 2022. **6**(12): p. 1399-1406.